Self-Encapsulated Doping of n-Type Graphene Transistors with Extended Air Stability

Po-Hsun Ho,[†] Yun-Chieh Yeh,[†] Di-Yan Wang,[†] Shao-Sian Li,[†] Hsin-An Chen,[†] Yi-Hsuan Chung,[†] Chih-Cheng Lin,[†] Wei-Hua Wang,[‡] and Chun-Wei Chen[†,*]

[†]Department of Materials Science and Engineering, National Taiwan University, Taipei 10617, Taiwan and [‡]Institute of Atomic and Molecular Sciences, Academia Sinica, Taipei 106, Taiwan

ABSTRACT

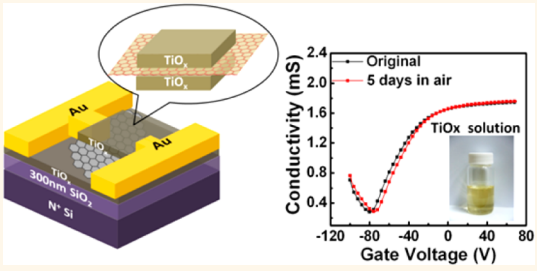

This paper presents an innovative approach to fabricating controllable n-type doping graphene transistors with extended air stability by using self-encapsulated doping layers of titanium suboxide (TiOx) thin films, which are an amorphous phase of crystalline TiO_2 and can be solution processed. The nonstoichiometry TiOx thin films consisting of a large number of oxygen vacancies exhibit several unique functions simultaneously in the n-type doping of graphene as an efficient electron-donating agent, an effective dielectric screening medium, and also an encapsulated layer. A novel device structure consisting of both top and bottom coverage of TiOx thin layers on a graphene transistor exhibited strong n-type transport characteristics with its Dirac point shifted up to −80 V and an enhanced electron mobility with doping. Most interestingly, an extended stability of the device without rapid degradation after doping was observed when it was exposed to ambient air for several days, which is not usually observed in other n-type doping methods in graphene. Density functional theory calculations were also employed to explain the observed unique n-type doping characteristics of graphene using TiOx thin films. The technique of using an "active" encapsulated layer with controllable and substantial electron doping on graphene provides a new route to modulate electronic transport behavior of graphene and has considerable potential for the future development of air-stable and large-area graphene-based nanoelectronics.

KEYWORDS: graphene · TiOx · n-type doping of graphene and transistor · air stability

Graphene, which consists of a single-atom-thick plane of carbon atoms arranged in a honeycomb lattice, has demonstrated excellent carrier transport attributed to a unique two-dimensional (2D) energy dispersion.[1−4] Because the entire layer of carbon atoms has an immediate exposure to the surroundings, tunable electrical properties of graphene in both n-type and p-type are attainable by instantaneous doping.[5−9] To date, several approaches have been applied to control the carrier types and modulate carrier concentrations in graphene by means of adsorption of molecules,[9−11] covalent functionalization,[12−17] surface modification of substrates,[18−20] or using metallic ultrathin films.[21−23] Because these doped graphene devices are usually vulnerable to the influence of the surrounding environment, the fundamental issues regarding doping, stability, and lifetime are crucial subjects for the development of graphene-based integrated electronics. In addition, the task to obtain a stable n-type graphene transistor at ambient condition is generally more difficult to achieve than its p-type counterpart. The conventional method to obtain electron-doped graphite is usually through alkali metal intercalation;[23] however, the rapid degradation upon exposure to air limits its practical applications. Several methods have been proposed to fabricate n-type graphene transistors; for example, substitutional doping with the incorporation of nitrogen dopants into carbon lattices under a vacuum condition can result in n-type transport of graphene.[15,16] The incorporation of nitrogen atoms into the matrix of the sp^2-bonded carbon usually leads to the appearance of nitrogen impurities, such as pyridine or pyrrole configurations,[16] which may increase the defect density and deteriorate the carrier mobilities of graphene.[14,17] Alternative methods to obtain n-type graphene transistors by using surface dopants of organic molecules,[24] polymers,[6] or metallic thin films[21−23] have also been reported recently. For example, McCreary *et al.* recently reported substantial n-type doping of graphene by depositing a submonolayer of metallic Ti using a molecular beam epitaxy system.[21] In addition, Romero *et al.*[25]

* Address correspondence to chunwei@ntu.edu.tw.

Received for review April 13, 2012 and accepted June 4, 2012.

Published online June 08, 2012
10.1021/nn301639j

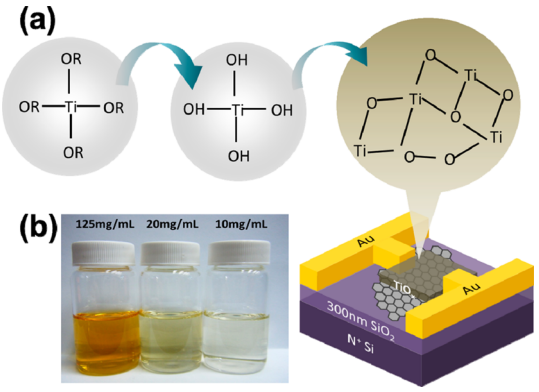

Figure 1. (a) Schematic representation of a graphene transistor covered with a TiOx thin layer using spin-coating. A brief flowchart of the steps involved in the preparations of the TiOx layer is also shown. (b) Photographic images of the TiOx sol–gel precursor solutions with concentrations of 125 mg/mL (original), diluted solutions of 20 and 10 mg/mL, respectively (from left to right).

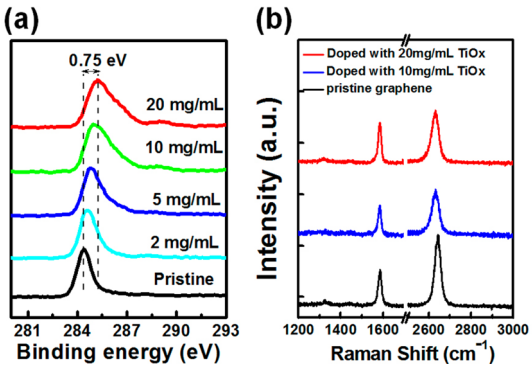

Figure 2. (a) XPS spectra of C1s peaks of graphene covered by TiOx thin layers resulting from various concentrations. (b) Raman spectroscopy measurement of graphene without and with coating of TiOx thin layers. The excitation wavelength was 633 nm.

demonstrated an n-type graphene field effect transistor on SiO_2/Si substrate under a very high vacuum condition (up to 5×10^{-7} Torr) by removing the residual gaseous molecules. However, these n-type graphene devices have very limited thermal and chemical stabilities and are usually sensitive to the influence of ambient environment. This study demonstrated an innovative approach to fabricate n-type graphene transistors with enhanced electron mobilities and also extended air stability by using self-encapsulated doping layers of titanium suboxide (TiOx) thin films, which are an amorphous phase of crystalline TiO_2 and can be solution processed.[26] The simultaneous doping and encapsulation layers of TiOx thin films on the graphene transistors results in substantial n-type doping of graphene with enhanced electron mobilities and also prevents the rapid degradation of devices influenced by the surrounding environment. The use of a solution-processable "active" encapsulated layer with controllable and substantial doping on graphene has a considerable potential to develop air-stable and large-area graphene-based electronic devices. The first-principles calculations based on density functional theory (DFT) calculations were also employed to investigate interfacial charge transfer, which explains the observed unique n-type doping characteristics of graphene using TiOx thin films.

RESULTS AND DISCUSSION

Figure 1a shows the schematic representation of the device structure of a graphene transistor covered with a TiOx thin layer using spin-coating. The precursor was converted to a TiOx thin film by hydrolysis when the TiOx precursor solution was spin-cast on top of the graphene layer and heated to 80 °C to dry the residual solvent in a glovebox for 10 min. The as-synthesized TiOx film was amorphous and transparent with an energy gap of approximately 3.91 eV (see Supporting Information) and was used as an effective electron-transporting layer and an optical spacer to enhance the efficiencies of polymer photovoltaics.[26,27] As revealed by the analysis of X-ray photoelectron spectroscopy (XPS) (see Supporting Information), an oxygen deficiency with a Ti/O ratio of 1:1.59 at the surface of the TiOx thin film was observed where the oxygen vacancies are usually formed during hydrolysis and condensation processes.[28] The sol–gel TiOx solutions with various concentrations (Figure 1b) were spin-coated on top of graphene transistors, followed by hydrolysis processes to form the doping layers.

We first used the Hall measurement to determine the carrier types of various graphene devices deposited on SiO_2/Si substrates (see Supporting Information). The pristine graphene device had p-type transporting carriers, which are mainly attributed to doping by adsorbate molecules on the SiO_2/Si substrates[25] when exposed to humidity and/or oxygen.[10,11] The carriers of devices immediately changed to n-type transporting carriers when the graphene devices were covered by TiOx thin films. Figure 2a shows the representative XPS spectra of C1s peaks of graphene with and without coating of TiOx thin layers. The binding energy of the C1s peak of the pristine graphene corresponding to pure sp^2-hybridized states was centered at 284.5 ± 0.05 eV. A gradual shift of C1s peaks toward higher binding energies with increased TiOx concentrations was observed after deposition of TiOx capping layers. The C1s peak shifted by approximately 0.75 eV at a concentration of 20 mg/mL of the TiOx capping layer. Further increase in the concentrations of the TiOx layers does not cause a further shift of C1s peaks but broadens their bandwidths. The observed energy shift may be explained by n-type doping of graphene upon TiOx deposition because of electron transfer at the TiOx/graphene interface, which moves the Fermi level toward or even higher than the Dirac point of graphene.[16,17] The n-type doping characteristics of graphene are further supported by the Raman spectroscopy measurement, as shown in Figure 2b. The 2D bands of graphene devices

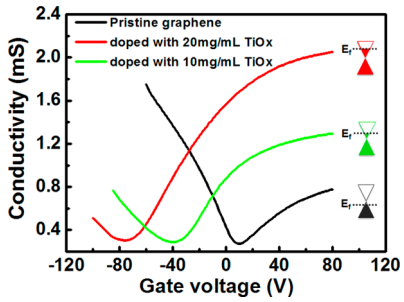

Figure 3. Gate-dependent conductivity (σ) of pristine graphene and graphene devices covered by TiOx thin films spin-coated from two different concentrations of 10 and 20 mg/mL. All of these devices were measured at a vacuum condition of 10^{-4} Torr.

covered by TiOx thin layers shifted down from 2644 cm^{-1} (pristine) to 2634 cm^{-1} (10 mg/mL) and 2632 cm^{-1} (20 mg/mL), due to the effect of the Fermi level shift on the phonon frequencies as a result of electron doping of graphene.[29] The intensity ratios of the I(2D)/I(G) also decreased with increased concentrations of TiOx thin layers. In addition, a decrease in the full width at half-maximum (fwhm) values of the G peaks from 18 cm^{-1} (pristine) to 16 cm^{-1} (10 mg/mL) and 15 cm^{-1}(20 mg/mL) occurred in conjunction with an increase in the fwhm values of the 2D peaks from 30 cm^{-1} (pristine) to 36 cm^{-1} (10 mg/mL) and 38 cm^{-1}-(20 mg/mL). All of these Raman spectroscopy results that the G peak stiffens and sharpens, the 2D peak shows a downshift, and the intensity ratio of the G and 2D peaks decreases are consistent with those observed in typical electron doping of graphene.[29,30] In addition, the D band intensities in the graphene devices covered by TiOx thin films were almost negligible, suggesting that this type of doping mainly occurs through surface charge transfer doping at TiOx/graphene interfaces and does not cause a substantial distortion of the local carbon lattices, as observed in covalently functionalizational[7,12,13] or substitutional[14−17] doping of graphene, in which an enhanced D band intensity with increased disorder after doping is usually observed.[12−15,17]

Figure 3 shows the gate-dependent conductivity (σ) of graphene transistor devices covered by TiOx thin films spin-coated from two different concentrations of 10 and 20 mg/mL. Electron and hole mobilities were extracted by measuring the slopes of the conductivity curves away from the Dirac points. For comparison, the pristine graphene transistor deposited on SiO_2/Si was also fabricated and exhibited typical p-type transporting behavior. After depositing TiOx thin films on the graphene devices, the Dirac points shifted toward negative gate voltages, representing typical n-type transport behavior as a result of TiOx thin films donating electrons to graphene. A clear trend toward a negative shift of the Dirac gate voltage was observed as the concentrations of the TiOx sol−gel solutions spin-coated on the graphene devices increased. The Dirac points for the graphene transistors with and without coating of TiOx thin layers were +10 V (pristine) and −41 V (10 mg/mL) and −76 V (20 mg/mL), and the corresponding carrier concentrations as estimated by $n = -\alpha(V_g - V_d)$, with $\alpha = 7.2 \times 10^{10}$ cm^{-2} V^{-1} (based on calculated capacitance values at zero gate bias), were $+7.2 \times 10^{11}$ cm^{-2} (pristine), -2.95×10^{12} cm^{-2} (10 mg/mL), and -5.47×10^{12} cm^{-2} (20 mg/mL). The hole mobilities of devices decreased with increased concentrations of TiOx thin layers from 2914 cm^2 V^{-1} s^{-1} (pristine) to 1513 cm^2 V^{-1} s^{-1} (10 mg/mL) and 1230 cm^2 V^{-1} s^{-1} (20 mg/mL). By contrast, no decline in electron mobilities was observed after depositing TiOx thin layers on graphene, and the electron mobilities of these samples increased from 1056 cm^2 V^{-1} s^{-1} (pristine) to 1955 cm^2 V^{-1} s^{-1} (10 mg/mL) and 2212 cm^2 V^{-1} s^{-1} (20 mg/mL). The similar asymmetric effects on electron and hole conduction of graphene after doping was also observed in the molecular doping of graphene, which was mainly caused by the neutrality point misalignment at the electrode/channel interface.[6] The enhanced electron mobilities of graphene covered by TiOx thin films with doping differed considerably from those obtained in the nitrogen substitutional doping of graphene, in which electron mobilities decreased after doping.[14,17] As shown in the Raman spectra in Figure 2b, a negligible D band signal was observed in the n-type doping of graphene covered by a TiOx thin layer, indicating that the scattering probability from the local defects and impurities of graphene introduced by the covalently bonded dopants may be substantially diminished in the surface charge transfer doping. In addition, dielectric screening may be another important factor to explain the enhanced electron mobility of graphene covered by a TiOx thin layer. It has been reported that the carrier mobilities of graphene on the SiO_2 substrate are substantially enhanced when the dielectric constants of top media increase,[31,32] which may minimize the charged impurity-induced long-range Coulomb scattering through dielectric screening. Therefore, the mobility limited by long-range impurity scattering increases by reducing the interaction of electrons with charged impurities because of the increased background dielectric. The TiOx thin film, which has a high dielectric constant of approximately 70−120,[33] may effectively reduce the scattering probability originating from the charge impurities through dielectric screening, which may explain the enhanced electron mobilities of graphene with TiOx doping. A more detailed investigation of the scattering mechanism of graphene covered by a TiOx thin layer is currently underway.

In addition to the top doping, we also investigated the bottom doping effect of graphene from substrate. Figure 4a shows the schematic device structure of graphene deposited on top of a precoated TiOx thin

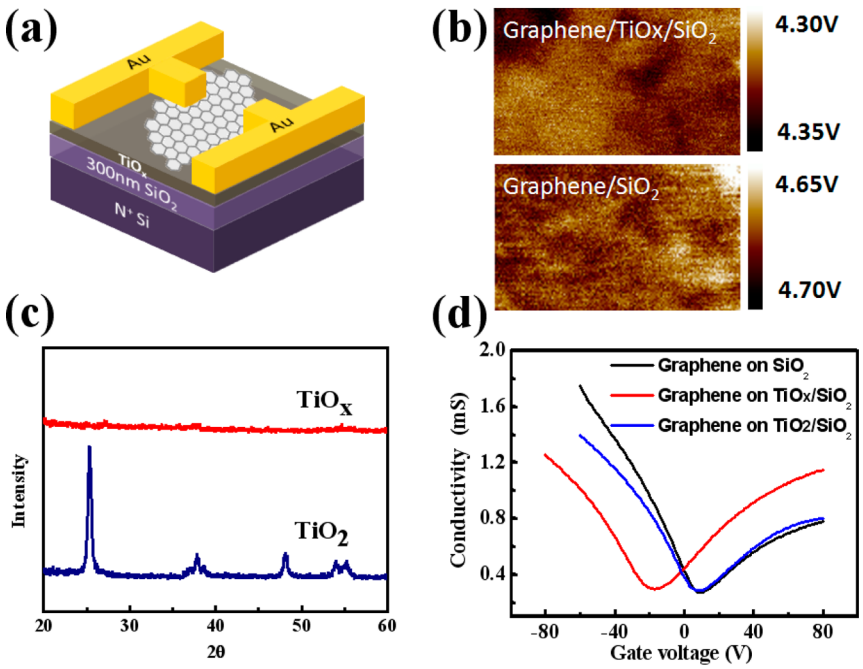

Figure 4. (a) Schematic device structure of graphene deposited on top of a precoated TiOx thin film (10 nm) on the SiO_2/Si substrate. (b) Work function mapping images of graphene deposited on top of a TiOx/SiO_2/Si (top) and SiO_2/Si substrate (bottom). (c) XRD patterns of amorphous TiOx and crystalline TiO_2 thin films. (d) Transport characteristic curves of graphene deposited on two different substrates of TiOx/SiO_2/Si and TiO_2/SiO_2/Si. The curve of graphene on SiO_2/Si is also shown as a reference. All of these devices were measured at a vacuum condition of 10^{-4} Torr.

film (10 nm) on SiO_2/Si substrate. Figure 4b shows the work function mapping images of graphene deposited on top of TiOx/SiO_2/Si and SiO_2/Si substrates revealed by a Kelvin probe microscope. The Fermi levels of graphene moved from the original ~4.68 eV on the SiO_2/Si substrate (bottom) to ~4.33 eV on the TiOx/SiO_2/Si substrate (top), indicating n-type doping[34] with electrons transferring from the TiOx substrate to graphene. The TiOx layer was deposited at room temperature and treated at 80 °C, which is far below the crystallization temperatures to the anatase or rutile phases of TiO_2 with a T_c >450 °C. We also investigated the doping characteristics of graphene on top of amorphous TiOx and crystalline TiO_2 thin films. Figure 4c shows the X-ray diffraction patterns of amorphous TiOx and crystalline TiO_2 after calcination at 500 °C, which shows a typical signature of the TiO_2 anatase phase. Similar to the graphene transistor capped by a TiOx thin layer, a typical n-type transport characteristic curve of graphene deposited on top of a precoated TiOx substrate was also observed, as shown in Figure 4d, with the Dirac point at approximately −21 V and hole and electron mobilities of 2185 and 1387 $cm^2 V^{-1} s^{-1}$, respectively. By contrast, the device of graphene deposited on top of the TiO_2 substrate after calcination exhibits the Dirac point at +8 V and hole and electron mobilities of 2534 and 1099 $cm^2 V^{-1} s^{-1}$, respectively. The transport behavior of graphene deposited on top of the TiO_2/SiO_2 substrate is quite similar to that of the pristine graphene device on the SiO_2 substrate, indicating that the amorphous TiOx thin film has a much stronger n-type doping effect on graphene compared to the crystalline TiO_2 counterpart.

To further verify the doping mechanism of graphene by a TiOx thin layer, we performed density functional theory (DFT) calculations to examine the charge transfer between graphene and two Ti-rich or O-rich surfaces of a TiO_2 crystal, as shown in Figure 5a,b, respectively. The magnitude of charge transfer in Figure 5b was magnified 10 times to obtain a clear comparison. Substantial electron transfer from Ti atoms to carbon atoms occurred at the interface between graphene and a Ti-rich TiO_2 surface, resulting in an increased electron density on the graphene surface with a shorter distance of approximately 2.3 Å between graphene and the Ti-rich surface. By contrast, a slight charge transfer between oxygen and carbon atoms at the interface of graphene and the O-rich TiO_2 surface (slight p-doping) caused larger separation of approximately 3 Å between two surfaces. Because a TiOx thin film has inherent oxygen deficiency, electron transfer is expected to occur from the TiOx thin film to graphene at their interfaces, resulting in n-type doping. This effect will be largely reduced when the TiOx thin film is transferred into the TiO_2 thin film. The result is also consistent with the recent reported substantial n-type doping of graphene by depositing a submonolayer of metallic Ti using a molecular beam epitaxy system; however, the effect of charge transfer was considerably reduced when the Ti was converted to TiO_2.[21] Therefore, the

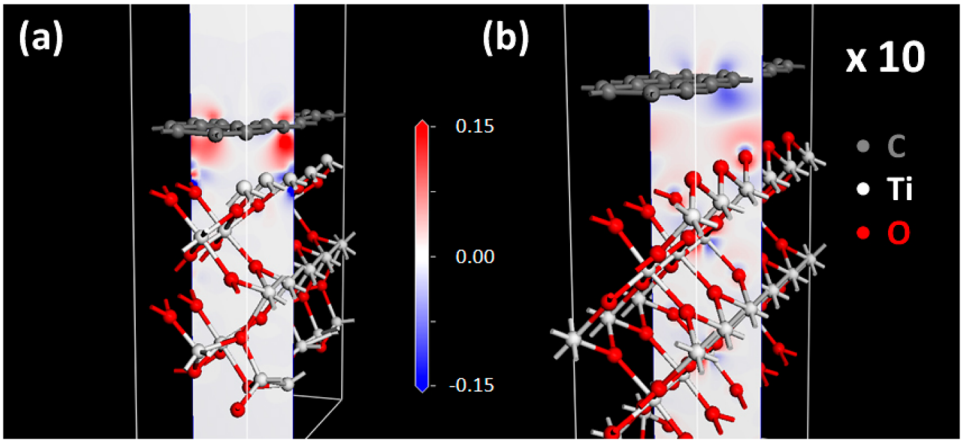

Figure 5. Density functional theory (DFT) calculations of charge transfer between graphene and (a) Ti-rich or (b) O-rich surfaces of a TiO_2 crystal. The red and blue parts indicate gain and loss of electron densities, respectively. The magnitude of charge transfer in (b) was magnified by 10 times.

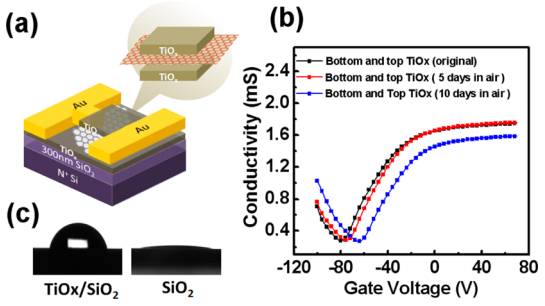

Figure 6. (a) Device structure consisting of both top and bottom coverage of TiOx thin layers on a graphene transistor. (b) Gate-dependent conductivity curves of the graphene transistor device consisting of both top and bottom coverage of a TiOx thin layer as they are exposed in air for 5 and 10 days. All of these measurements were performed in ambient air. The average humidity in laboratory environment during the measurement period was around 70%. (c) Measured contact angles of a typical SiO_2/Si substrate and a TiOx/SiO_2/Si substrate were 7 and 76°, respectively.

nonstoichiometric TiOx thin films, which consist of a large number of oxygen vacancies, act as a stable electron-donating material of graphene made from solution processes.

We thus proposed a device structure consisting of both top and bottom coverage of TiOx thin layers on a graphene transistor, as shown in Figure 6a, where the concentration of the TiOx solution used for spin-coating was 20 mg/mL. It was found that the graphene device sandwiched by both sides of TiOx thin layers has the Dirac voltage at −80 V, and the electron mobility was largely enhanced with a value of 3430 $cm^2 V^{-1} s^{-1}$. In addition, we found that this device consisting of both top- and bottom-covered TiOx doping layers exhibited similar mobility values when it was measured in ambient air or in a vacuum condition. To further test the stability of the device when it was exposed to ambient air, we kept the device in the laboratory environment for 5 and 10 days and also measured its current−voltage characteristics in the ambient air, as shown in Figure 6b. The device exhibited no substantial degradation after 5 days of exposure in the ambient condition with only a small shift of the Dirac voltage (from −80 to −78 V) and the electron mobility of approximately 3343 $cm^2 V^{-1} s^{-1}$. After 10 days of exposure in ambient air, the device showed a Dirac voltage of −62 V with the electron mobility of approximately 2790 $cm^2 V^{-1} s^{-1}$. This result of extended stability of graphene was not commonly seen in many other graphene transistors because they were usually very sensitive to the influence by the surrounding environment. We found that it was necessary to cover both sides of the graphene by TiOx thin films to obtain good encapsulation because the Dirac voltage of the device covered with only the top TiOx layer exhibited a large shift from −76 to −51 V after 3 days of exposure in air (see Supporting Information). It is well-known that the SiO_2 substrate is hydrophilic because of the dangling bonds of the Si and SiOH groups on the surface, which may attract the polar molecules (*e.g.*, water), resulting in a typical p-type doping of graphene.[10,25] The contact angles of the bare SiO_2/Si substrate and the TiOx/SiO_2/Si substrate were 7 and 76°, respectively, as shown in Figure 6c. Because the TiOx thin film after hydrolysis demonstrated a more hydrophobic surface property,[28] this may effectively reduce the influence of water molecules on the substrate. The adsorbate molecules through attachment on the SiO_2 substrate surface may cause instability and degradation of the device without the insertion of the bottom TiOx layer. Therefore, an n-type graphene transistor with extended air stability and enhanced electron mobility can be achieved in conjunction with both top- and bottom-encapsulated doping layers of TiOx thin films.

CONCLUSIONS

In summary, we demonstrated a controllable n-type graphene transistor with extended air stability by using

solution-processable TiOx thin films, which have both functions of doping and encapsulation simultaneously. Further development in the fabrication of pn junctions of graphene devices using self-encapsulated doping layers offers considerable potential for the development of graphene-based integrated circuits.

EXPERIMENTAL SECTION

Synthesis of TiOx. TiOx was synthesized *via* sol−gel[26] procedures as follows: 2-methoxyethanol ($CH_3OCH_2CH_2OH$, Acros, 99+%) and ethanolamine ($H_2NCH_2CH_2OH$, Acros, 99%) were first mixed in a three-necked flask, and titanium(IV) isopropoxide ($Ti[OCH(CH_3)_2]_4$, Acros, 98+%) was thus injected after stirring for 10 min. The temperature was then raised to 80 °C and kept for 2 h, followed by heating to 120 °C for 1 h. The heating cycle was repeated until the orange color appeared. The original concentration of as-synthesized TiOx gel was 125 mg/mL. The precursor solutions with various concentrations were prepared by mixing with *n*-butanol ($CH_3CH_2CH_2CH_2OH$, Acros, 99%) to form the diluted solutions.

Preparations of Graphene. Chemical vapor deposition (CVD) was used for the growth of graphene on copper foil.[35] A polycrystalline Cu foil (purchased from Nilaco Inc.) was placed on a hot wall furnace consisting of a 1.5 in. fused silica tube. The furnace was then heated to 950 °C. Typically, a reduction process was conducted in H_2 flow for ~30 min prior to the introduction of CH_4. With H_2 flow, CH_4 was then introduced for graphene growth with a flow rate of 10/50 sccm H_2/CH_4 for 10 min. After a growth time of 15 min, CH_4 was then shut off and the system was cooled in H_2 or Ar flow to reach room temperature. The entire procedures were conducted at low pressure (typically ~500 mTorr during the growth stage).

Fabrications of Graphene Transistors Covered with TiOx. Silicon dioxide (SiO_2) thin films with a thickness of 300 nm deposited on heavily doped silicon wafers with a capacitance of 10.8 nF cm^{-2} were used in all of the device fabrications. For the transfer of graphene, we used the roll-to-roll production method[36] to transfer the graphene films on top of SiO_2/Si substrates. The source and drain electrodes (Au/Cr) were fabricated by utilizing thermal evaporation through a shadow mask with a channel length of 100 μm and a channel width of 1200 μm. The sol−gel TiOx solutions with different concentrations were thus spin-coated on top of graphene transistors followed by hydrolysis processes to form the self-encapsulated doping layers. For the fabrication of a graphene transistor with bottom doping, a precoated TiOx thin layer with a thickness of 10 nm was deposited on top of the SiO_2/Si substrate. Afterward, the depositions of graphene and source−drain electrodes were fabricated with the similar procedures.

Measurements and Characterizations. X-ray photoemission spectroscopy (XPS) spectra were obtained using a VG Scientific ESCALAB 250 system. X-ray source was generated from the Al target (1486.8 eV) with a pass energy of 20 eV, and the take-off angle for the collection of photoelectrons was 90° from the surface normal. Hall measurement was performed on the whole area of the graphene device by using an ECOPIA HMS-3000 system. The XRD measurement was performed by Bruker D8 tools advance, operating with Cu Kα radiation (λ = 1.5406 Å) generated at 40 keV and 40 mA. The Raman measurement was conducted using a 633 nm He−Ne laser as an excitation source and recorded by a HORIBA iHR 550 spectrometer equipped with a Symphony CCD detector. Contact angles of Milli-Q ultrapure water droplets (Milli-Q, ρ > 18 MΩ·cm, Millipore) were measured by a contact angle goniometer (Sindatek Model 100SB) at ambient condition. All measured contact angles were advancing angles. The work function mapping images of graphene were determined by using scanning Kelvin probe microscopy (SKPM) (Innova, Vecco Inc.). Cyclic voltammetry (CV) experiments were performed in a three-electrode electrochemical cell by using an Autolab PGSTAT302N potentiostat/galvanostat. The gate-dependent conductivities of the films were measured with a probe station at room temperature under a vacuum condition of 10^{-4} Torr or in ambient condition. The details of density functional calculations to investigate charge transfer and electronic structures at graphene/TiOx interface are described in the Supporting Information.

Conflict of Interest: The authors declare no competing financial interest.

Acknowledgment. This work is supported by National Science Council, Taiwan, for the project of "Core facilities of novel graphene based materials" (Project Nos. NSC 100-2119-M-002-020 and 100-2628-M-002-013-MY3). The authors would also like to thank Professor Che-Chen Chang and Mr. Hsiu-Wei Cheng from Precision Instrumentation Center, National Taiwan University, for technical support of XPS.

Supporting Information Available: Additional experimental details. This material is available free of charge *via* the Internet at http://pubs.acs.org.

REFERENCES AND NOTES

1. Novoselov, K. S.; Geim, A. K.; Morozov, S. V.; Jiang, D.; Zhang, Y.; Dubonos, S. V.; Grigorieva, I. V.; Firsov, A. A. Electric Field Effect in Atomically Thin Carbon Films. *Science* **2004**, *306*, 666–669.
2. Geim, A. K. Graphene: Status and Prospects. *Science* **2009**, *324*, 1530–1534.
3. Zhang, Y.; Tan, Y.-W.; Stormer, H. L.; Kim, P. Experimental Observation of the Quantum Hall Effect and Berry's Phase in Graphene. *Nature* **2005**, *438*, 201–204.
4. Novoselov, K. S.; Geim, A. K.; Morozov, S. V.; Jiang, D.; Katsnelson, M. I.; Grigorieva, I. V.; Dubonos, S. V.; Firsov, A. A. Two-Dimensional Gas of Massless Dirac Fermions in Graphene. *Nature* **2005**, *438*, 197–200.
5. Chen, W.; Chen, S.; Qi, D. C.; Gao, X. Y.; Wee, A. T. S. Surface Transfer p-Type Doping of Epitaxial Graphene. *J. Am. Chem. Soc.* **2007**, *129*, 10418–10422.
6. Farmer, D. B.; Golizadeh-Mojarad, R.; Perebeinos, V.; Lin, Y.-M.; Tulevski, G. S.; Tsang, J. C.; Avouris, P. Chemical Doping and Electron−Hole Conduction Asymmetry in Graphene Devices. *Nano Lett.* **2009**, *9*, 388–392.
7. Wang, X.; Li, X.; Zhang, L.; Yoon, Y.; Weber, P. K.; Wang, H.; Guo, J.; Dai, H. N-Doping of Graphene through Electrothermal Reactions with Ammonia. *Science* **2009**, *324*, 768–771.
8. Chen, Z.; Santoso, I.; Wang, R.; Xie, L. F.; Mao, H. Y.; Huang, H.; Wang, Y. Z.; Gao, X. Y.; Chen, Z. K.; Ma, D.; *et al.* Surface Transfer Hole Doping of Epitaxial Graphene Using MoO_3 Thin Film. *Appl. Phys. Lett.* **2010**, *96*, 213104.
9. Schedin, F.; Geim, A. K.; Morozov, S. V.; Hill, E. W.; Blake, P.; Katsnelson, M. I.; Novoselov, K. S. Detection of Individual Gas Molecules Adsorbed on Graphene. *Nat. Mater.* **2007**, *6*, 652–655.
10. Ryu, S.; Liu, L.; Berciaud, S.; Yu, Y.-J.; Liu, H.; Kim, P.; Flynn, G. W.; Brus, L. E. Atmospheric Oxygen Binding and Hole Doping in Deformed Graphene on a SiO_2 Substrate. *Nano Lett.* **2010**, *10*, 4944–4951.
11. Yang, Y.; Murali, R. Binding Mechanisms of Molecular Oxygen and Moisture to Graphene. *Appl. Phys. Lett.* **2011**, *98*, 093116.
12. Niyogi, S.; Bekyarova, E.; Itkis, M. E.; Zhang, H.; Shepperd, K.; Hicks, J.; Sprinkle, M.; Berger, C.; Lau, C. N.; deHeer, W. A.; *et al.* Spectroscopy of Covalently Functionalized Graphene. *Nano Lett.* **2010**, *10*, 4061–4066.
13. Englert, J. M.; Dotzer, C.; Yang, G.; Schmid, M.; Papp, C.; Gottfried, J. M.; Steinrück, H.-P.; Spiecker, E.; Hauke, F.; Hirsch, A. Covalent Bulk Functionalization of Graphene. *Nat. Chem.* **2011**, *3*, 279–286.

14. Lin, Y.-C.; Lin, C.-Y.; Chiu, P.-W. Controllable Graphene N-Doping with Ammonia Plasma. *Appl. Phys. Lett.* **2010**, *96*, 133110–133110-3.
15. Guo, B.; Liu, Q.; Chen, E.; Zhu, H.; Fang, L.; Gong, J. R. Controllable N-Doping of Graphene. *Nano Lett.* **2010**, *10*, 4975–4980.
16. Usachov, D.; Vilkov, O.; Grüneis, A.; Haberer, D.; Fedorov, A.; Adamchuk, V. K.; Preobrajenski, A. B.; Dudin, P.; Barinov, A.; Oehzelt, M.; *et al.* Nitrogen-Doped Graphene: Efficient Growth, Structure, and Electronic Properties. *Nano Lett.* **2011**, *11*, 5401–5407.
17. Wei, D.; Liu, Y.; Wang, Y.; Zhang, H.; Huang, L.; Yu, G. Synthesis of N-Doped Graphene by Chemical Vapor Deposition and Its Electrical Properties. *Nano Lett.* **2009**, *9*, 1752–1758.
18. Wang, R.; Wang, S.; Zhang, D.; Li, Z.; Fang, Y.; Qiu, X. Control of Carrier Type and Density in Exfoliated Graphene by Interface Engineering. *ACS Nano* **2010**, *5*, 408–412.
19. Lafkioti, M.; Krauss, B.; Lohmann, T.; Zschieschang, U.; Klauk, H.; Klitzing, K. v.; Smet, J. H. Graphene on a Hydrophobic Substrate: Doping Reduction and Hysteresis Suppression under Ambient Conditions. *Nano Lett.* **2010**, *10*, 1149–1153.
20. Wang, Y. y.; Ni, Z. h.; Yu, T.; Shen, Z. X.; Wang, H. m.; Wu, Y. h.; Chen, W.; Shen Wee, A. T. Raman Studies of Monolayer Graphene: The Substrate Effect. *J. Phys. Chem. C* **2008**, *112*, 10637–10640.
21. McCreary, K. M.; Pi, K.; Kawakami, R. K. Metallic and Insulating Adsorbates on Graphene. *Appl. Phys. Lett.* **2011**, *98*, 192101-3.
22. Pi, K.; McCreary, K. M.; Bao, W.; Han, W.; Chiang, Y. F.; Li, Y.; Tsai, S. W.; Lau, C. N.; Kawakami, R. K. Electronic Doping and Scattering by Transition Metals on Graphene. *Phys. Rev. B* **2009**, *80*, 075406.
23. Chen, J. H.; Jang, C.; Adam, S.; Fuhrer, M. S.; Williams, E. D.; Ishigami, M. Charged-Impurity Scattering in Graphene. *Nat. Phys.* **2008**, *4*, 377–381.
24. Yu, W. J.; Liao, L.; Chae, S. H.; Lee, Y. H.; Duan, X. Toward Tunable Band Gap and Tunable Dirac Point in Bilayer Graphene with Molecular Doping. *Nano Lett.* **2011**, *11*, 4759–4763.
25. Romero, H. E.; Shen, N.; Joshi, P.; Gutierrez, H. R.; Tadigadapa, S. A.; Sofo, J. O.; Eklund, P. C. n-Type Behavior of Graphene Supported on Si/SiO_2 Substrates. *ACS Nano* **2008**, *2*, 2037–2044.
26. Kim, J. Y.; Kim, S. H.; Lee, H. H.; Lee, K.; Ma, W.; Gong, X.; Heeger, A. J. New Architecture for High-Efficiency Polymer Photovoltaic Cells Using Solution-Based Titanium Oxide as an Optical Spacer. *Adv. Mater.* **2006**, *18*, 572–576.
27. Park, S. H.; Roy, A.; Beaupre, S.; Cho, S.; Coates, N.; Moon, J. S.; Moses, D.; Leclerc, M.; Lee, K.; Heeger, A. J. Bulk Heterojunction Solar Cells with Internal Quantum Efficiency Approaching 100%. *Nat. Photonics* **2009**, *3*, 297–302.
28. Cho, S.; Lee, K.; Heeger, A. J. Extended Lifetime of Organic Field-Effect Transistors Encapsulated with Titanium Sub-Oxide as an `Active' Passivation/Barrier Layer. *Adv. Mater.* **2009**, *21*, 1941–1944.
29. Das, A.; Pisana, S.; Chakraborty, B.; Piscanec, S.; Saha, S. K.; Waghmare, U. V.; Novoselov, K. S.; Krishnamurthy, H. R.; Geim, A. K.; Ferrari, A. C.; *et al.* Monitoring Dopants by Raman Scattering in an Electrochemically Top-Gated Graphene Transistor. *Nat. Nanotechnol.* **2008**, *3*, 210–215.
30. Frank, O.; Mohr, M.; Maultzsch, J.; Thomsen, C.; Riaz, I.; Jalil, R.; Novoselov, K. S.; Tsoukleri, G.; Parthenios, J.; Papagelis, K.; *et al.* Raman 2D-Band Splitting in Graphene: Theory and Experiment. *ACS Nano* **2011**, *5*, 2231–2239.
31. Chen, F.; Xia, J.; Ferry, D. K.; Tao, N. Dielectric Screening Enhanced Performance in Graphene FET. *Nano Lett.* **2009**, *9*, 2571–2574.
32. Jang, C.; Adam, S.; Chen, J. H.; Williams, E. D.; Das Sarma, S.; Fuhrer, M. S. Tuning the Effective Fine Structure Constant in Graphene: Opposing Effects of Dielectric Screening on Short- and Long-Range Potential Scattering. *Phys. Rev. Lett.* **2008**, *101*, 146805.
33. van Dover, R. B. Amorphous Lanthanide-Doped TiOx Dielectric Films. *Appl. Phys. Lett.* **1999**, *74*, 3041–3043.
34. Yu, Y.-J.; Zhao, Y.; Ryu, S.; Brus, L. E.; Kim, K. S.; Kim, P. Tuning the Graphene Work Function by Electric Field Effect. *Nano Lett.* **2009**, *9*, 3430–3434.
35. Li, X.; Cai, W.; An, J.; Kim, S.; Nah, J.; Yang, D.; Piner, R.; Velamakanni, A.; Jung, I.; Tutuc, E.; *et al.* Large-Area Synthesis of High-Quality and Uniform Graphene Films on Copper Foils. *Science* **2009**, *324*, 1312–1314.
36. Bae, S.; Kim, H.; Lee, Y.; Xu, X.; Park, J.-S.; Zheng, Y.; Balakrishnan, J.; Lei, T.; Ri Kim, H.; Song, Y. I.; *et al.* Roll-to-Roll Production of 30-Inch Graphene Films for Transparent Electrodes. *Nat. Nanotechnol.* **2010**, *5*, 574–578.